### Title
Deep Search for Decaying Dark Matter with XMM-Newton Blank-Sky Observations




### Journal
Physical Review Letters, 127(5)

### ISSN
0031-9007



### Authors
Foster, Joshua W
Kongsore, Marius
Dessert, Christopher
et al.



### Publication Date
2021-07-30

### DOI
10.1103/physrevlett.127.051101

Peer reviewed

# Deep Search for Decaying Dark Matter with *XMM-Newton* Blank-Sky Observations

Joshua W. Foster,[1,2,3,*] Marius Kongsore,[1] Christopher Dessert,[1,2,3] Yujin Park,[1,2,3]
Nicholas L. Rodd,[2,3] Kyle Cranmer,[4] and Benjamin R. Safdi[2,3,†]

[1]*Leinweber Center for Theoretical Physics, Department of Physics, University of Michigan, Ann Arbor, Michigan 48109, USA*
[2]*Berkeley Center for Theoretical Physics, University of California, Berkeley, California 94720, USA*
[3]*Theoretical Physics Group, Lawrence Berkeley National Laboratory, Berkeley, California 94720, USA*
[4]*Center for Cosmology and Particle Physics, New York University, New York, New York 10003, USA*

Sterile neutrinos with masses in the keV range are well-motivated extensions to the Standard Model that could explain the observed neutrino masses while also making up the dark matter (DM) of the universe. If sterile neutrinos are DM then they may slowly decay into active neutrinos and photons, giving rise to the possibility of their detection through narrow spectral features in astrophysical x-ray data sets. In this Letter, we perform the most sensitive search to date for this and other decaying DM scenarios across the mass range from 5 to 16 keV using archival *XMM-Newton* data. We reduce 547 Ms of data from both the MOS and PN instruments using observations taken across the full sky and then use this data to search for evidence of DM decay in the ambient halo of the Milky Way. We determine the instrumental and astrophysical baselines with data taken far away from the Galactic Center, and use Gaussian process modeling to capture additional continuum background contributions. No evidence is found for unassociated x-ray lines, leading us to produce the strongest constraints to date on decaying DM in this mass range.

Sterile-neutrino dark matter (DM) is a well-motivated DM candidate that may give rise to observable nearly monochromatic x-ray signatures [1–3]. In this scenario the DM has a mass in the keV range and may decay into an active neutrino and an x ray, with energy set by half the rest mass of the sterile neutrino [4]. Sterile-neutrino DM is motivated in part by the seesaw mechanism for explaining the active neutrino masses [5,6]. In this Letter we present one of the most sensitive searches for sterile-neutrino DM, along with other DM candidates that may decay to monochromatic x rays, over the mass range $m_\chi \in [5, 16]$ keV. We do so by searching for DM decay from the ambient halo of the Milky Way using all archival data from the *XMM-Newton* telescope collected from its launch until September 5, 2018.

This work builds heavily upon the method developed in Dessert *et al.* [7], which used *XMM-Newton* blank-sky observations (BSOs) to strongly disfavor the decaying DM explanation of the previously observed 3.5 keV unidentified x-ray line (UXL). This UXL was found in nearby galaxies and clusters [8–12]. However the analysis performed in Dessert *et al.* [7] was able to robustly rule out the DM decay rate required to explain the previous 3.5 keV UXL signals [13]. (For additional nonobservations, see Refs. [14–20].) We extend the search in Dessert *et al.* [7] to the broader mass range $m_\chi \in [5, 16]$, and in doing so implement the following notable differences: (i) we use a data-driven approach to construct stacked, background-subtracted data sets in rings around the Galactic Center (GC), while Ref. [7] performed a joint-likelihood analysis at the level of individual exposures, and (ii) we use Gaussian process (GP) modeling to describe continuum residuals, instead of parametric modeling as used in [7].

As demonstrated in Dessert *et al.* [7], BSO searches for DM decaying in the Milky Way halo can be both more sensitive and more robust than extra-galactic searches, because (i) the expected DM flux, even at angles $\sim 45°$ away from the GC, rivals the expected flux from the most promising extra-galactic objects, such as M31 and the Perseus cluster; (ii) promising extra-galactic targets have continuum and linelike x-ray features that are confounding backgrounds for DM searches (dwarf galaxies being an exception [18,21]), while BSOs instead focus on the lowest-background regions of the sky; (iii) extra-galactic targets require pointed observations, while in principle any observation collected by *XMM-Newton* is sensitive to DM decay in the Milky Way, opening up considerably more exposure time.

The limits presented in this Letter represent the strongest found using the *XMM-Newton* instrument over the energy range $\sim$2.5–8 keV. At higher energies our limits are superseded by those found using the *NuSTAR* satellite [22–26]. Reference [24] performed a search similar in spirit to that in this work (though with *NuSTAR*) in that they looked for DM decay from the Milky Way halo near the GC

(∼10° away in their case), while Ref. [26] searched for DM decay from M31 with *NuSTAR*.

Our results put in tension efforts to explain the abundance of DM with sterile neutrinos. For example, in the Neutrino Minimal Standard Model ($\nu$MSM) [27–29], which may simultaneously explain the observed neutrino masses, DM density, and baryon asymmetry, the Standard Model is supplemented by three heavier sterile-neutrino states, the lightest of which is the DM candidate. The DM abundance is generated through the mixing of sterile and active neutrinos [1], which can further be resonantly enhanced by a finite lepton chemical potential [2,29–35], though other production mechanisms are also possible [3,36,37]. DM models such as axionlike particle DM [38] and moduli DM [39] predict similar UXL signatures from DM decay.

*Data reduction and processing.*—We process and analyze all publicly available data collected before 5 September 2018 by the metal oxide semiconductor (MOS) and positive–negative (PN) cameras on board *XMM-Newton*. We subject each exposure to a set of quality cuts, which are described shortly. Those exposures satisfying the quality cuts are included in our angularly binned data products. In particular, we divide the sky into 30 concentric annuli centered around the GC, each with a width of 6° in angular radius from the GC, $r_{\rm GC}$, where $\cos(r_{\rm GC}) = \cos(l)\cos(b)$ in terms of the Galactic longitude $l$ and latitude $b$. We label these from 1 to 30, starting from the innermost ring. We further mask the Galactic plane such that we only include the region $|b| \geq 2°$. In each ring we then produce stacked spectra where, in each energy bin, we sum the counts from each exposure whose central position lies within that annulus. We produce separate data sets for the MOS and PN cameras, which have 2400 and 4096 energy channels, respectively. In addition to stacking the counts in each ring and energy channel, we also construct the appropriately weighted detector response matrices in every ring for forward modeling an incident astrophysical flux. The full-sky maps and associated modeling data are provided as supplementary data [40] in both the annuli and in finer-resolution hierarchical equal area isolatitude pixelation binning [41]. We analyze the MOS data from 2.5 to 8 keV and the PN data from 2.5 to 7 keV, in order to exclude intervals containing large instrumental features.

*Data analysis.*—Having constructed our data in all 30 rings, we divide the full sky into two regions of interest (ROI): a signal ROI, consisting of annuli 1 through 8 ($0° \leq r_{\rm GC} \leq 48°$ with $|b| \geq 2°$), inclusive, and the background ROI, consisting of annuli 20 through 30 ($114° \leq r_{\rm GC} \leq 180°$ with $|b| \geq 2°$). The regions are illustrated in Fig. 1. The MOS (PN) exposure time in the signal ROI is 25.27 Ms (5.56 Ms), whereas in the background ROI it is 62.51 Ms (17.54 Ms). The signal flux is proportional to the $D$ factor, which is defined by the line-of-sight integral of the Galactic DM density $\rho_{\rm DM}$,

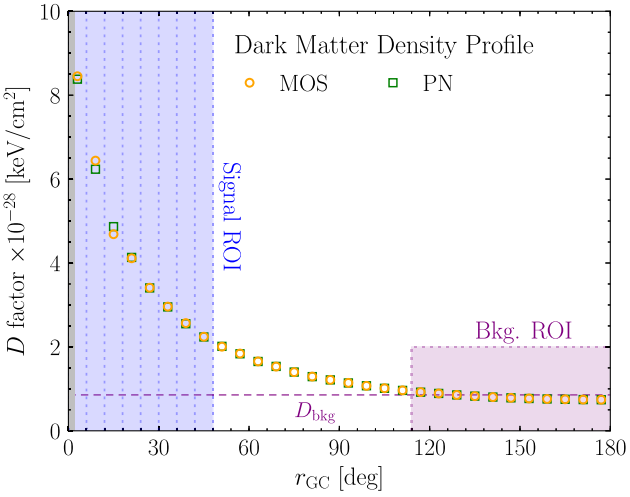


FIG. 1. Our fiducial $D$ factor, which is proportional to the expected DM signal flux. Values are given in all 30 annuli, which are 6° wide in angular distance from the GC (with $|b| > 2°$), and we define a signal and background ROI as shown. In each ring, we compute the $D$ factor of all MOS or PN exposures, weighted according to the observation time and field of view. The horizontal line indicates $D_{\rm bkg}$, the mean $D$ factor in the background ROI.

$D \equiv \int ds \rho_{\rm DM}$. In Fig. 1 we show the appropriately weighted $D$ factor in each annuli. The motivation for the two ROIs is that the signal should dominate in the inner regions of the Galaxy and become progressively weaker further away from the GC. The background ROI is chosen to be large enough to have significantly more exposure time than the signal ROI, so that using the background-subtracted data does not significantly broaden the statistical uncertainties. We stack the data over the full background ROI, which has the $D$ factor $D_{\rm bkg}$, and use this as an estimate of the instrumental and astrophysical baseline fluxes by subtracting this data from the data in each ring of the signal ROI. This subtraction mostly removes large instrumental lines, as illustrated in the Supplemental Material [42], Fig. S1.

We analyze the background-subtracted data in each annulus for evidence of a UXL. The data is modeled as a combination of narrow spectral features at the locations of known astrophysical and instrumental lines, and a continuum flux which we account for using GP modeling. Note that the instrumental lines need not be completely removed by the data-subtraction procedure, leaving a residual flux or flux deficit that must be modeled. Astrophysical emission lines from the Milky Way plasma should be brighter in the signal ROI, and so are also expected to appear in the background-subtracted data. For both astrophysical and instrumental lines, the lines are modeled using the forward modeling matrices for MOS and PN. We allow the instrumental lines to have either positive or negative normalizations, while the astrophysical lines are restricted

to having positive normalizations. To decide which lines to include in our residual background model we start with an initial list of known instrumental and astrophysical lines. The instrumental lines are determined from an analysis of the background ROI data, while the astrophysical lines are those expected to be produced by the Milky Way. In each ring, and for MOS and PN independently, we then determine the significance of each emission line, keeping those above $\sim 2\sigma$. As a result, every ring has a different set of lines included in the analysis. We note that it is conceivable that a UXL might be inadvertently removed by an overly subtracted instrumental line at the same energy; however, it would be highly unlikely for such a conspiracy to occur in every ring, given the varying $D$ factor. The effects of subthreshold instrumental lines are mitigated through a *spurious-signal* nuisance parameter [56], as discussed in the Supplemental Material [42].

The unprecedented data volume incorporated into this analysis necessitates a flexible approach to modeling the residual continuum emission, which is accomplished with GP modeling, in order to minimize background mismodeling. As opposed to parametric modeling, where the model is specified by a specific functional form and associated list of model parameters, GP modeling is nonparametric: the model expectations for the data at two different energies, $E$ and $E'$, are assumed to be normally distributed with nontrivial covariance. Taking the model expectation to have zero mean, the GP model is then fully specified by the covariance kernel, $K(E, E')$. We model the mean-subtracted data using the nonstationary kernel $K(E, E') = A_{\rm GP} \exp[-(E - E')^2/(2EE'\sigma_E^2)]$, implemented in GEORGE [57], where $\sigma_E$ is the correlation-length hyperparameter and $A_{\rm GP}$ is the amplitude hyperparameter. We fix $\sigma_E$ such that it is larger than the energy resolution of the detector, which is $\delta E/E \sim 0.03$ across most energies for MOS and PN, while ensuring $\sigma_E$ is kept small enough to have the flexibility to model real variations in the data. The goal is to balance two competing effects. If $\sigma_E$ approaches the lower limit imposed by the energy resolution of the detector, then the GP model would have the flexibility to account for linelike features, which would reduce our sensitivity when searching for such features over the continuum background. On the other hand, if $\sigma_E$ is too large then the GP continuum model may not accurately model real small-scale variations in the data. In our fiducial analysis we fix $\sigma_E = 0.3$, though in the Supplemental Material [42] we show that our results are robust to variations not only in this choice, but also to modifications to the form of the kernel itself. In contrast, the hyperparameter $A_{\rm GP}$ is treated as a nuisance parameter that is profiled over when searching for UXLs.

We then follow the statistical approach developed in Frate *et al.* [58], which used GP modeling to perform an improved search for narrow resonances over a continuum background in the context of the Large Hadron Collider. In particular, we construct a likelihood ratio $\Lambda$ between the model with and without the signal component, where the signal is the UXL line at fixed energy $E_{\rm sig}$. The null model is as above, the combination of a GP model with a single nuisance parameter $A_{\rm GP}$, and a set of background lines, whose amplitudes are treated as nuisance parameters. We use the marginal likelihood from the GP fit in the construction of the likelihood ratio [58]. Note that as the number of counts in all energy bins is large ($\gg 100$), we are justified in assuming normally distributed errors in the context of the GP modeling. We then profile over all nuisance parameters. Finally, the discovery significance is quantified by the test statistic (TS) $t = -2 \ln \Lambda$. We verify explicitly in the Supplemental Material [42] that under the null hypothesis $t$ follows a $\chi^2$ distribution. The 95% one-sided upper limits are constructed from the profile likelihood, as a function of the signal amplitude.

We implement this procedure and scan for a UXL from 2.5 to 8 keV in 5 eV intervals. At each test point we construct profile likelihoods for signal flux independently for each ring using the background-subtracted MOS and PN data. We then combine the likelihoods between rings—and eventually cameras—in a joint likelihood in the context of the DM model, as discussed shortly. As an example, Fig. 2 illustrates the signal and null model fits to the innermost MOS background-subtracted signal-annulus data for a putative UXL at 3.5 keV (indicated by the vertical dashed line). Note that while the fit is performed over the full energy range (2.5–8 keV) for clarity we show the data enlarged to the range 3 to 4 keV. In this case the data have a deficit, which manifests itself as a signal with a negative amplitude.

*DM interpretation.*—We combine together the profile likelihoods from the individual annuli to test the decaying DM model. In the context of sterile-neutrino DM with mass $m_\chi$ and mixing angle $\theta$, the DM decay in the Galactic halo produces an x-ray flux at energy $m_\chi/2$ that scales as $\Phi \propto m_\chi^4 D \sin^2(2\theta)$ [59]. Note that the $D$ factors, appropriately averaged over observations in the individual annuli, are

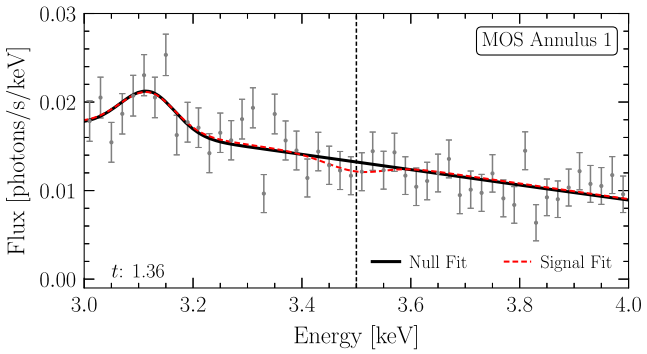


FIG. 2. The background-subtracted MOS data for the innermost annulus, downbinned by a factor of 4 for presentation purposes. The indicated best-fit null and signal models, for a 3.5 keV UXL, are constructed using the GP modeling described in the text.

illustrated in Fig. 1. Thus, at a fixed DM mass $m_\chi$ we may construct profile likelihoods as functions of $\sin^2(2\theta)$ to appropriately combine the profile likelihoods as functions of flux in the individual annuli. We subtract $D_{\rm bkg}$ from the $D$ factors in each signal ring since any UXL would also appear in the background ROI and thus be included in the background subtraction.

The $D$ factors may be computed from the DM density profile of the Milky Way. Modern hydrodynamic cosmological simulations indicate that the DM density profile in Milky Way mass halos generally have a high degree of spherical symmetry (for a review, see Ref. [60]). Further, the presence of baryons contracts the inner ∼10 kpc of the profile away from the canonical Navarro, Frenk, and White (NFW) DM distribution [61,62], so that there is an enhancement of the DM density at smaller radii versus the NFW expectation [63–68], though cores could develop on top of this contraction at radii $\lesssim$2 kpc [69–72]. For example, in Milky Way analog halos within the Fire-2 simulations the DM-only and hydrodynamic simulations produce DM density profiles that agree within ∼25% at 10 kpc, but with baryons the density profiles are typically around twice as large as the NFW DM-only expectation at distances ∼1 kpc away from the GC [67]. To be conservative we assume the canonical NFW density profile for all radii, though in the Supplemental Material [42] we discuss how our results change for alternate density profiles.

The NFW profile is specified by a characteristic density $\rho_0$ and a scale radius $r_s$: $\rho_{\rm DM}(r) = \rho_0/(r/r_s)/(1+r/r_s)^2$. We use the recent results from Cautun *et al.* [73], who combined *Gaia* DR2 Galactic rotation curve data [74] with total mass estimates for the Galaxy from satellite observations [75,76]. These data imply, in the context of the NFW model, a virial halo mass $M_{200}^{\rm DM} = 0.82^{+0.09}_{-0.18} \times 10^{12}\ M_\odot$ and a concentration $c = r_{200}/r_s = 13.31^{+3.60}_{-2.68}$, with a nontrivial covariance between $M_{200}^{\rm DM}$ and $c$ [73] such that lower concentrations prefer higher halo masses. Within the 2D 68% containment region for $M_{200}^{\rm DM}$ and $c$ quoted in Ref. [73], the lowest DM density at $r \approx 0.5$ kpc, and thus the most conservative profile for the present analysis, is obtained for $\rho_0 = 6.6 \times 10^6\ M_\odot/{\rm kpc}^3$ and $r_s = 19.1$ kpc. We adopt these values for our fiducial analysis. With our choice of NFW DM parameters the local DM density, at the solar radius, is ∼0.29 GeV/ cm$^3$ (cf. 0.4 GeV/ cm$^3$ used in Dessert *et al.* [7]), which is consistent with local measurements of the DM density using the vertical motion of tracer stars perpendicular to the Galactic plane (see, e.g., Refs. [77,78]).

We search for evidence of decaying DM in 10 eV intervals with mass 5–16 keV, masking 0.1 keV windows around the locations of known lines, as indicated in Fig. 3. We construct the joint likelihoods for the MOS and PN data sets. We test and account for additional background mismodeling in the MOS and PN analyses by looking at the distribution of best-fit mixing angles in the energy sidebands, using a technique similar to the "spurious signal" used by the ATLAS collaboration in the search for the Higgs boson [56]. This procedure is described in the Supplemental Material [42] and only has a small effect at low masses. We then combine, at a given mass, the resulting MOS and PN profile likelihoods to obtain the final profile likelihood used to construct the limit and discovery significance shown in Fig. 3. In that figure we show the one-sided 95% upper limit on $\sin^2(2\theta)$ in the upper panel, along with the 1 and 2$\sigma$ expectations for the power-constrained upper limit [79] under the null hypothesis (shaded green and gold, respectively).

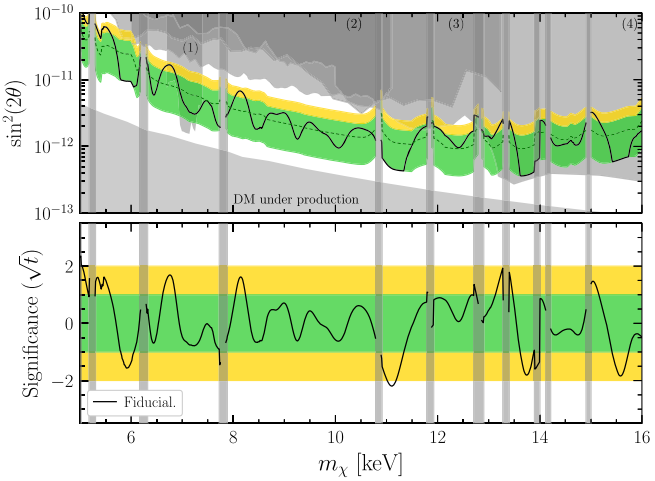


FIG. 3. Upper panel: the power-constrained 95% upper limit on the DM lifetime from this work, presented in the context of the sterile-neutrino mixing angle $\sin^2(2\theta)$, as a function of the DM mass $m_\chi$. The dark grey regions correspond to theoretical bounds for DM underproduction in the $\nu$MSM or bounds from previous x-ray searches (1)–(5); see text for details. Lower panel: the associated sign-weighted significance for the UXL. Vertical grey regions denote background lines and are at least partially masked. Green and gold regions indicate $1/2\sigma$ expectations under the null hypothesis. These results are shown in the context of more general DM models as constraints on the DM lifetime in the Supplemental Material [42], Fig. S6.

We find no evidence for decaying DM signals above our predetermined significance threshold of 5$\sigma$ global significance (corresponding to ∼6$\sigma$ local significance), as shown in the bottom panel. In that figure we compare our upper limit to previous limits in the literature, adjusted to our fiducial DM model for the Milky Way where appropriate. In the context of the $\nu$MSM it is impossible to explain all of the observed DM in the region marked "DM under production" because of the big bang nucleosynthesis bound on the lepton chemical potential [30–32]. Note that the $\nu$MSM also predicts that the DM becomes increasingly warm for decreasing $m_\chi$, which leads to tension with Milky Way satellite galaxy counts for low $m_\chi$: data from the Dark Energy Survey and other Galactic

satellite surveys [80] constrain $m_\chi$ greater than ∼15–20 keV in the $\nu$MSM [81] (which can be strengthened further when combined with strong lensing measurements [82]), though we note that our results apply to more general DM production mechanisms that do not predict modifications to small-scale structure. In Fig. 3 we also show previous x-ray limits from (1) Dessert *et al.* [7], (2) a *Chandra* search for DM decay in the Milky Way [83], (3) a *Chandra* search for DM decay in M31 [14], and (4) combined *NuSTAR* searches for DM decay: in the Milky Way [22–24], the Bullet Cluster [25], and M31 [26]. Note that the results from Milky Way searches have been adjusted to use the same DM density profile as in our fiducial analysis.

*Discussion.*—We find no significant evidence for decaying DM, which leads us to set some of the strongest constraints to date on the DM lifetime. We confirm the results of Dessert *et al.* [7] for the nonobservation of a DM decay line near 3.5 keV using a more robust and flexible analysis strategy, leaving little room for a decaying DM explanation of the previously observed 3.5 keV anomalies [8–12]. (See the Supplemental Material [42] for further discussion.)

Given the data volume incorporated into this analysis it is unlikely that further analyses of *XMM-Newton* data, or *Chandra* data, could produce qualitatively stronger results on the DM lifetime in the mass range considered here. However, the approach taken in this Letter may lead to a powerful advancement in discovery power with future data sets from surveys such as those by the upcoming *Athena* [84] and *XRISM* [85] telescopes. A combination of the data collected by those missions and the analysis framework introduced in this Letter may lead to the discovery of decaying DM in the few-keV mass range at lifetimes beyond those probed in this Letter.

The supporting data for this article are openly available from [40].

We thank Kerstin Perez and Christoph Weniger for useful conversations. This work was supported in part by the DOE Early Career Grant No. DESC0019225. This research used resources from the National Energy Research Scientific Computing Center (NERSC) and the Lawrencium computational cluster provided by the IT Division at the Lawrence Berkeley National Laboratory, supported by the Director, Office of Science, and Office of Basic Energy Sciences, of the U.S. Department of Energy under Contract No. DE-AC02-05CH11231. N. L. R. is supported by the Miller Institute for Basic Research in Science at the University of California, Berkeley. K. C. is partially supported by NSF Grant No. PHY-1505463m; NSF Grants No. ACI-1450310, No. OAC-1836650, and No. OAC-1841471; and the Moore-Sloan Data Science Environment at NYU.

*fosterjw@umich.edu
†brsafdi@lbl.gov

[1] S. Dodelson and L. M. Widrow, Sterile-Neutrinos As Dark Matter, Phys. Rev. Lett. **72**, 17 (1994).
[2] X.-D. Shi and G. M. Fuller, A New Dark Matter Candidate: Nonthermal Sterile Neutrinos, Phys. Rev. Lett. **82**, 2832 (1999).
[3] A. Kusenko, Sterile Neutrinos, Dark Matter, and the Pulsar Velocities in Models with a Higgs Singlet, Phys. Rev. Lett. **97**, 241301 (2006).
[4] P. B. Pal and L. Wolfenstein, Radiative decays of massive neutrinos, Phys. Rev. D **25**, 766 (1982).
[5] T. Yanagida, Horizontal symmetry and masses of neutrinos, Prog. Theor. Phys. **64**, 1103 (1980).
[6] R. N. Mohapatra and G. Senjanovic, Neutrino Mass and Spontaneous Parity Violation, Phys. Rev. Lett. **44**, 912 (1980).
[7] C. Dessert, N. L. Rodd, and B. R. Safdi, The dark matter interpretation of the 3.5-keV line is inconsistent with blank-sky observations, Science **367**, 1465 (2020).
[8] E. Bulbul, M. Markevitch, A. Foster, R. K. Smith, M. Loewenstein, and S. W. Randall, Detection of an unidentified emission line in the stacked x-ray spectrum of galaxy clusters, Astrophys. J. **789**, 13 (2014).
[9] A. Boyarsky, O. Ruchayskiy, D. Iakubovskyi, and J. Franse, Unidentified Line in X-Ray Spectra of the Andromeda Galaxy and Perseus Galaxy Cluster, Phys. Rev. Lett. **113**, 251301 (2014).
[10] O. Urban, N. Werner, S. W. Allen, A. Simionescu, J. S. Kaastra, and L. E. Strigari, A Suzaku search for dark matter emission lines in the x-ray brightest galaxy clusters, Mon. Not. R. Astron. Soc. **451**, 2447 (2015).
[11] T. E. Jeltema and S. Profumo, Discovery of a 3.5 keV line in the Galactic Centre and a critical look at the origin of the line across astronomical targets, Mon. Not. R. Astron. Soc. **450**, 2143 (2015).
[12] N. Cappelluti, E. Bulbul, A. Foster, P. Natarajan, M. C. Urry, M. W. Bautz, F. Civano, E. Miller, and R. K. Smith, Searching for the 3.5 keV line in the deep fields with Chandra: The 10 Ms observations, Astrophys. J. **854**, 179 (2018).
[13] C. Dessert, N. L. Rodd, and B. R. Safdi, Response to a comment on Dessert "The dark matter interpretation of the 3.5 keV line is inconsistent with blank-sky observations", Phys. Dark Universe **30**, 100656 (2020).
[14] S. Horiuchi, P. J. Humphrey, J. Onorbe, K. N. Abazajian, M. Kaplinghat, and S. Garrison-Kimmel, Sterile neutrino dark matter bounds from galaxies of the Local Group, Phys. Rev. D **89**, 025017 (2014).
[15] D. Malyshev, A. Neronov, and D. Eckert, Constraints on 3.55 keV line emission from stacked observations of dwarf spheroidal galaxies, Phys. Rev. D **90**, 103506 (2014).
[16] M. E. Anderson, E. Churazov, and J. N. Bregman, Non-detection of x-ray emission from sterile neutrinos in stacked galaxy spectra, Mon. Not. R. Astron. Soc. **452**, 3905 (2015).
[17] T. Tamura, R. Iizuka, Y. Maeda, K. Mitsuda, and N. Y. Yamasaki, An x-ray spectroscopic search for dark matter in the perseus cluster with Suzaku, Publ. Astron. Soc. Jpn. **67**, 23 (2015).

[18] T. E. Jeltema and S. Profumo, Deep XMM observations of Draco rule out at the 99% confidence level a dark matter decay origin for the 3.5 keV Line, Mon. Not. R. Astron. Soc. **458**, 3592 (2016).

[19] F. A. Aharonian *et al.* (Hitomi Collaboration), *Hitomi* constraints on the 3.5 keV line in the Perseus galaxy cluster, Astrophys. J. **837**, L15 (2017).

[20] A. Gewering-Peine, D. Horns, and J. H. M. M. Schmitt, A sensitive search for unknown spectral emission lines in the diffuse X-ray background with XMM-Newton, J. Cosmol. Astropart. Phys. 06 (2017) 036.

[21] O. Ruchayskiy, A. Boyarsky, D. Iakubovskyi, E. Bulbul, D. Eckert, J. Franse, D. Malyshev, M. Markevitch, and A. Neronov, Searching for decaying dark matter in deep XMM–Newton observation of the Draco dwarf spheroidal, Mon. Not. R. Astron. Soc. **460**, 1390 (2016).

[22] A. Neronov, D. Malyshev, and D. Eckert, Decaying dark matter search with NuSTAR deep sky observations, Phys. Rev. D **94**, 123504 (2016).

[23] K. Perez, K. C. Y. Ng, J. F. Beacom, C. Hersh, S. Horiuchi, and R. Krivonos, Almost closing the $\nu$MSM sterile neutrino dark matter window with NuSTAR, Phys. Rev. D **95**, 123002 (2017).

[24] B. M. Roach, K. C. Y. Ng, K. Perez, J. F. Beacom, S. Horiuchi, R. Krivonos, and D. R. Wik, NuSTAR Tests of Sterile-Neutrino Dark Matter: New Galactic Bulge Observations and Combined Impact, Phys. Rev. D **101**, 103011 (2020).

[25] S. Riemer-Sørensen *et al.*, Dark matter line emission constraints from NuSTAR observations of the Bullet Cluster, Astrophys. J. **810**, 48 (2015).

[26] K. C. Y. Ng, B. M. Roach, K. Perez, J. F. Beacom, S. Horiuchi, R. Krivonos, and D. R. Wik, New Constraints on Sterile Neutrino Dark Matter from *NuSTAR* M31 Observations, Phys. Rev. D **99**, 083005 (2019).

[27] T. Asaka, S. Blanchet, and M. Shaposhnikov, The nuMSM, dark matter and neutrino masses, Phys. Lett. B **631**, 151 (2005).

[28] T. Asaka and M. Shaposhnikov, The $\nu$MSM, dark matter and baryon asymmetry of the universe, Phys. Lett. B **620**, 17 (2005).

[29] L. Canetti, M. Drewes, T. Frossard, and M. Shaposhnikov, Dark matter, baryogenesis and neutrino oscillations from right handed neutrinos, Phys. Rev. D **87**, 093006 (2013).

[30] A. D. Dolgov, S. H. Hansen, S. Pastor, S. T. Petcov, G. G. Raffelt, and D. V. Semikoz, Cosmological bounds on neutrino degeneracy improved by flavor oscillations, Nucl. Phys. **B632**, 363 (2002).

[31] P. D. Serpico and G. G. Raffelt, Lepton asymmetry and primordial nucleosynthesis in the era of precision cosmology, Phys. Rev. D **71**, 127301 (2005).

[32] A. Boyarsky, O. Ruchayskiy, and M. Shaposhnikov, The role of sterile neutrinos in cosmology and astrophysics, Annu. Rev. Nucl. Part. Sci. **59**, 191 (2009).

[33] M. Laine and M. Shaposhnikov, Sterile neutrino dark matter as a consequence of nuMSM-induced lepton asymmetry, J. Cosmol. Astropart. Phys. 06 (2008) 031.

[34] T. Venumadhav, F.-Y. Cyr-Racine, K. N. Abazajian, and C. M. Hirata, Sterile neutrino dark matter: Weak interactions in the strong coupling epoch, Phys. Rev. D **94**, 043515 (2016).

[35] J. F. Cherry and S. Horiuchi, Closing in on resonantly produced sterile neutrino dark matter, Phys. Rev. D **95**, 083015 (2017).

[36] K. Petraki and A. Kusenko, Dark-matter sterile neutrinos in models with a gauge singlet in the Higgs sector, Phys. Rev. D **77**, 065014 (2008).

[37] K. N. Abazajian and A. Kusenko, Hidden treasures: Sterile neutrinos as dark matter with miraculous abundance, structure formation for different production mechanisms, and a solution to the $\sigma_8$ problem, Phys. Rev. D **100**, 103513 (2019).

[38] T. Higaki, K. Sik Jeong, and F. Takahashi, The 7 keV axion dark matter and the X-ray line signal, Phys. Lett. B **733**, 25 (2014).

[39] A. Kusenko, M. Loewenstein, and T. T. Yanagida, Moduli dark matter and the search for its decay line using Suzaku X-ray telescope, Phys. Rev. D **87**, 043508 (2013).

[40] J. Foster, M. Kongsore, C. Dessert, Y. Park, N. Rod, K. Cranmer, and B. Safdi, "Processed blank-sky data from the XMM-Newton Space Telescope," https://github.com/bsafdi/XMM_BSO_DATA.

[41] K. M. Gorski, E. Hivon, A. J. Banday, B. D. Wandelt, F. K. Hansen, M. Reinecke, and M. Bartelman, HEALPix—A Framework for high resolution discretization, and fast analysis of data distributed on the sphere, Astrophys. J. **622**, 759 (2005).

[42] See Supplemental Material at http://link.aps.org/supplemental/10.1103/PhysRevLett.127.051101 for further descriptions of the main methods, systematic tests, and additional results, which includes Refs. [43–55].

[43] Users Guide to the XMM-Newton Science Analysis System, Issue 14.0, 2018 (ESA: XMM-Newton SOC).

[44] D. H. Lumb, R. S. Warwick, M. Page, and A. De Luca, X-ray background measurements with xmm-newton epic, Astron. Astrophys. **389**, 93 (2002).

[45] G. Cowan, K. Cranmer, E. Gross, and O. Vitells, Asymptotic formulae for likelihood-based tests of new physics, Eur. Phys. J. C **71**, 1554 (2011); **73**, 2501(E) (2013).

[46] J. de Plaa, N. Werner, A. Simionescu, J. S. Kaastra, Y. G. Grange, and J. Vink, Cold fronts and multi-temperature structures in the core of Abell 2052, Astron. Astrophys. **523**, A81 (2010).

[47] A. Leccardi and S. Molendi, Radial temperature profiles for a large sample of galaxy clusters observed with xmm-newton*, Astron. Astrophys. **486**, 359 (2008).

[48] A. Foster, R. K. Smith, N. S. Brickhouse, and X. Cui, AtomDB and PyAtomDB: Atomic Data and Modelling Tools for High Energy and Non-Maxwellian Plasmas, in *American Astronomical Society Meeting Abstracts #227*, American Astronomical Society Meeting Abstracts, Vol. 227 (2016), p. 211.08.

[49] K. Koyama *et al.*, Iron and nickel line diagnostics for the galactic center diffuse emission, Publ. Astron. Soc. Jpn. **59**, S245 (2007).

[50] M. Ackermann *et al.* (Fermi-LAT Collaboration), Search for gamma-ray spectral lines with the fermi large area telescope

and dark matter implications, Phys. Rev. D **88**, 082002 (2013).
[51] A. Albert, G. A. Gomez-Vargas, M. Grefe, C. Munoz, C. Weniger, E. D. Bloom, E. Charles, M. N. Mazziotta, and A. Morselli (Fermi-LAT Collaboration), Search for 100 MeV to 10 GeV $\gamma$-ray lines in the Fermi-LAT data and implications for gravitino dark matter in $\mu\nu$SSM, J. Cosmol. Astropart. Phys. 10 (2014) 023.
[52] M. Ackermann *et al.* (Fermi-LAT Collaboration), Updated search for spectral lines from Galactic dark matter interactions with pass 8 data from the Fermi Large Area Telescope, Phys. Rev. D **91**, 122002 (2015).
[53] A. Boyarsky, D. Malyshev, O. Ruchayskiy, and D. Savchenko, Technical comment on the paper of Dessert "The dark matter interpretation of the 3.5 keV line is inconsistent with blank-sky observations", arXiv: 2004.06601.
[54] K. N. Abazajian, Technical Comment on "The dark matter interpretation of the 3.5-keV line is inconsistent with blank-sky observations", arXiv:2004.06170.
[55] A. Boyarsky, D. Iakubovskyi, O. Ruchayskiy, and D. Savchenko, Surface brightness profile of the 3.5 keV line in the Milky Way halo, arXiv:1812.10488.
[56] G. Aad *et al.* (ATLAS Collaboration), Measurement of Higgs boson production in the diphoton decay channel in pp collisions at center-of-mass energies of 7 and 8 TeV with the ATLAS detector, Phys. Rev. D **90**, 112015 (2014).
[57] S. Ambikasaran, D. Foreman-Mackey, L. Greengard, D. W. Hogg, and M. O'Neil, Fast Direct Methods for Gaussian Processes, (2014).
[58] M. Frate, K. Cranmer, S. Kalia, A. Vandenberg-Rodes, and D. Whiteson, Modeling smooth backgrounds and generic localized signals with Gaussian processes, arXiv: 1709.05681.
[59] P. B. Pal and L. Wolfenstein, Radiative decays of massive neutrinos, Phys. Rev. D **25**, 766 (1982).
[60] M. Vogelsberger, F. Marinacci, P. Torrey, and E. Puchwein, Cosmological Simulations of Galaxy Formation, Nat. Rev. Phys. **2**, 42 (2020).
[61] J. F. Navarro, C. S. Frenk, and S. D. M. White, The structure of cold dark matter halos, Astrophys. J. **462**, 563 (1996).
[62] J. F. Navarro, C. S. Frenk, and S. D. M. White, A Universal density profile from hierarchical clustering, Astrophys. J. **490**, 493 (1997).
[63] O. Y. Gnedin, A. V. Kravtsov, A. A. Klypin, and D. Nagai, Response of dark matter halos to condensation of baryons: Cosmological simulations and improved adiabatic contraction model, Astrophys. J. **616**, 16 (2004).
[64] M. Schaller, C. S. Frenk, R. G. Bower, T. Theuns, A. Jenkins, J. Schaye, R. A. Crain, M. Furlong, C. Dalla Vecchia, and I. G. McCarthy, Baryon effects on the internal structure of $\Lambda$CDM haloes in the EAGLE simulations, Mon. Not. R. Astron. Soc. **451**, 1247 (2015).
[65] Q. Zhu, F. Marinacci, M. Maji, Y. Li, V. Springel, and L. Hernquist, Baryonic impact on the dark matter distribution in Milky Way-sized galaxies and their satellites, Mon. Not. R. Astron. Soc. **458**, 1559 (2016).
[66] A. A. Dutton, A. V. Macciò, A. Dekel, L. Wang, G. S. Stinson, A. Obreja, A. Di Cintio, C. B. Brook, T. Buck, and X. Kang, NIHAO IX: The role of gas inflows and outflows in driving the contraction and expansion of cold dark matter haloes, Mon. Not. R. Astron. Soc. **461**, 2658 (2016).
[67] P. F Hopkins *et al.*, FIRE-2 simulations: Physics versus numerics in galaxy formation, Mon. Not. R. Astron. Soc. **480**, 800 (2018).
[68] M. R. Lovell *et al.*, The fraction of dark matter within galaxies from the IllustrisTNG simulations, Mon. Not. R. Astron. Soc. **481**, 1950 (2018).
[69] T. K. Chan, D. Kereš, J. Oñorbe, P. F. Hopkins, A. L. Muratov, C. A. Faucher-Giguère, and E. Quataert, The impact of baryonic physics on the structure of dark matter haloes: The view from the FIRE cosmological simulations, Mon. Not. R. Astron. Soc. **454**, 2981 (2015).
[70] P. Mollitor, E. Nezri, and R. Teyssier, Baryonic and dark matter distribution in cosmological simulations of spiral galaxies, Mon. Not. R. Astron. Soc. **447**, 1353 (2015).
[71] M. Portail, O. Gerhard, C. Wegg, and M. Ness, Dynamical modelling of the galactic bulge and bar: The Milky Way's pattern speed, stellar and dark matter mass distribution, Mon. Not. R. Astron. Soc. **465**, 1621 (2017).
[72] A. Lazar, J. S. Bullock, M. Boylan-Kolchin, T. K. Chan, P. F. Hopkins, A. S. Graus, A. Wetzel, K. El-Badry, C. Wheeler, M. C. Straight, D. Kereš, C.-A. Faucher-Giguère, A. Fitts, and S. Garrison-Kimmel, A dark matter profile to model diverse feedback-induced core sizes of $\Lambda$CDM haloes, Mon. Not. R. Astron. Soc. **497**, 2393 (2020).
[73] M. Cautun, A. Benítez-Llambay, A. J. Deason, C. S. Frenk, A. Fattahi, F. A. Gómez, R. J. J. Grand, K. A. Oman, J. F. Navarro, and C. M. Simpson, The milky way total mass profile as inferred from Gaia DR2, Mon. Not. R. Astron. Soc. **494**, 4291 (2020).
[74] A.-C. Eilers, D. W. Hogg, H.-W. Rix, and M. K. Ness, The Circular Velocity Curve of the Milky Way from 5 to 25 kpc, Astrophys. J. **871**, 120 (2019).
[75] L. L. Watkins, R. P. van der Marel, S. Tony Sohn, and N. Wyn Evans, Evidence for an intermediate-mass Milky Way from Gaia DR2 halo globular cluster motions, Astrophys. J. **873**, 118 (2019).
[76] T. M. Callingham, M. Cautun, A. J. Deason, C. S. Frenk, W. Wang, F. A. Gómez, R. J. J. Grand, F. Marinacci, and R. Pakmor, The mass of the Milky Way from satellite dynamics, Mon. Not. R. Astron. Soc. **484**, 5453 (2019).
[77] J. I. Read, The local dark matter density, J. Phys. G **41**, 063101 (2014).
[78] P. F. de Salas and A. Widmark, Dark matter local density determination: Recent observations and future prospects, arXiv:2012.11477.
[79] G. Cowan, K. Cranmer, E. Gross, and O. Vitells, Power-constrained limits, arXiv:1105.3166.
[80] A. Drlica-Wagner *et al.* (DES Collaboration), Milky Way Satellite Census. I. The observational selection function for Milky Way satellites in DES Y3 and Pan-STARRS DR1, Astrophys. J. **893**, 47 (2020).
[81] E. O. Nadler *et al.* (DES Collaboration), Milky Way Satellite Census. III. Constraints on Dark Matter Properties

from Observations of Milky Way Satellite Galaxies, Phys. Rev. Lett. **126**, 091101 (2021).

[82] E. O. Nadler, S. Birrer, D. Gilman, R. H. Wechsler, X. Du, A. Benson, A. M. Nierenberg, and T. Treu, Dark matter constraints from a unified analysis of strong gravitational lenses and Milky Way satellite galaxies, arXiv:2101.07810.

[83] D. Sicilian, N. Cappelluti, E. Bulbul, F. Civano, M. Moscetti, and C. S. Reynolds, Probing the Milky Way's Dark Matter halo for the 3.5 keV line, Astrophys. J. **905**, 146 (2020).

[84] X. Barcons, K. Nandra, D. Barret, J. W. den Herder, A. C. Fabian, L. Piro, and M. G. Watson (Athena Team), Athena: The X-ray observatory to study the hot and energetic Universe, J. Phys. Conf. Ser. **610**, 012008 (2015).

[85] Science with the X-ray imaging and spectroscopy mission (XRISM), arXiv:2003.04962.